AIP Journal of Applied Physics

Interfacial band alignment and structural properties of nanoscale TiO2 thin films for integration with epitaxial crystallographic oriented germanium

N. Jain, Y. Zhu, D. Maurya, R. Varghese, S. Priya, and M. K. Hudait

Citation: Journal of Applied Physics **115**, 024303 (2014); doi: 10.1063/1.4861137
View online: http://dx.doi.org/10.1063/1.4861137
View Table of Contents: http://scitation.aip.org/content/aip/journal/jap/115/2?ver=pdfcov
Published by the AIP Publishing

Interfacial band alignment and structural properties of nanoscale TiO_2 thin films for integration with epitaxial crystallographic oriented germanium

N. Jain,[1] Y. Zhu,[1] D. Maurya,[2] R. Varghese,[2] S. Priya,[2] and M. K. Hudait[1,a)]
[1]*Advanced Devices & Sustainable Energy Laboratory (ADSEL), Bradley Department of Electrical and Computer Engineering, Virginia Tech, Blacksburg, Virginia 24061, USA*
[2]*Center for Energy Harvesting Materials and Systems (CEHMS), Virginia Tech, Blacksburg, Virginia 24061, USA*

(Received 9 September 2013; accepted 16 December 2013; published online 10 January 2014)

We have investigated the structural and band alignment properties of nanoscale titanium dioxide (TiO_2) thin films deposited on epitaxial crystallographic oriented Ge layers grown on (100), (110), and (111)A GaAs substrates by molecular beam epitaxy. The TiO_2 thin films deposited at low temperature by physical vapor deposition were found to be amorphous in nature, and high-resolution transmission electron microscopy confirmed a sharp heterointerface between the TiO_2 thin film and the epitaxially grown Ge with no traceable interfacial layer. A comprehensive assessment on the effect of substrate orientation on the band alignment at the TiO_2/Ge heterointerface is presented by utilizing x-ray photoelectron spectroscopy and spectroscopic ellipsometry. A band-gap of 3.33 ± 0.02 eV was determined for the amorphous TiO_2 thin film from the Tauc plot. Irrespective of the crystallographic orientation of the epitaxial Ge layer, a sufficient valence band-offset of greater than 2 eV was obtained at the TiO_2/Ge heterointerface while the corresponding conduction band-offsets for the aforementioned TiO_2/Ge system were found to be smaller than 1 eV. A comparative assessment on the effect of Ge substrate orientation revealed a valence band-offset relation of $\Delta E_V(100) > \Delta E_V(111) > \Delta E_V(110)$ and a conduction band-offset relation of $\Delta E_C(110) > \Delta E_C(111) > \Delta E_C(100)$. These band-offset parameters are of critical importance and will provide key insight for the design and performance analysis of TiO_2 for potential high-κ dielectric integration and for future metal-insulator-semiconductor contact applications with next generation of Ge based metal-oxide field-effect transistors. © *2014 AIP Publishing LLC*.
[http://dx.doi.org/10.1063/1.4861137]

I. INTRODUCTION

New material innovation and their introduction in novel device architectures are at the forefront of continuing the miniaturization of the next generation of complimentary-metal-oxide-semiconductor (CMOS) integrated circuits. Germanium (Ge) as transistor channel material for post silicon (Si) CMOS era has regained considerable attention owing to its higher mobility for both electrons (2-fold) and holes (4-fold) as compared to Si.[1–3] The higher intrinsic carrier mobility in Ge can provide a larger drive current while the smaller band-gap could enable low voltage operation. However, one of the critical obstacles towards realization of high performance Ge metal-oxide semiconductor field-effect transistors (MOSFETs)[4–6] has been the passivation of Ge interface. Unlike Si, which offers a stable native oxide (SiO_2), the Ge native oxide is thermally unstable and soluble in water[7] which in turn leads to poor gate control and high gate leakage current. Thus, the down-selection of a robust surface passivation scheme accompanied with an optimal high-κ gate dielectric with sufficient band-offsets (>1 eV)[8–10] to Ge has been one of the biggest impediments in the realization of high performance Ge MOSFET devices. For comparing the relative advantages of various gate dielectrics, the figure of merit, f, must take into account the direct-tunneling limited gate leakage density and is represented by $f = \kappa\sqrt{\phi_b}$, where κ is the dielectric constant of the gate dielectric and ϕ_b is the tunnel barrier height.[11] Thus, it is evident from the aforementioned relation that it is of key significance to investigate high-κ gate dielectrics which have sufficient band-offsets with respect to Ge in order to efficiently suppress the gate leakage currents. In addition, another key challenge for the realization of high performance n-channel Ge MOSFETs has been the formation of low resistance ohmic contact to n-type Ge which is essential to achieve high drive current. The Fermi level pinning close to the Ge valence band edge at the metal/Ge junction[12,13] results in a large electron Schottky barrier, which in turn translates to a high specific contact resistivity to n-type Ge. It has been demonstrated that thin tunneling barriers with low conduction band-offset (CBO or ΔEc) to Ge could achieve higher currents and thus enable low resistance metal-insulator-semiconductor (MIS) contacts to Ge.[16] The insertion of such thin tunnel barriers including Al_2O_3,[14] SiN_3,[15] TiO_2,[16] and ZnO (Ref. 17) to form MIS contacts has been shown to reduce the Schottky barrier height as well as facilitate the unpinning of Fermi-level in n-type Ge.

Owing to its interesting optical, electrical, and chemical properties, titanium dioxide (TiO_2) is a promising material for multitude of applications including MIS contact,[16] photo-catalytic phenomenon,[18] solar energy conversion,[19] production of molecular hydrogen from water,[20] self-cleaning

a)Author to whom correspondence should be addressed. Electronic mail: mantu.hudait@vt.edu. Tel.: (540) 231-6663. Fax: (540) 231-3362.

process,[21] anti-reflection coating,[21] white pigment in paints,[22] gas sensors,[23] etc. Recently, the application base for TiO_2 has been growing rapidly, in particular due to its promising properties at nanoscale. Although there have been few reports on the investigation of TiO_2 as a potential high-κ gate dielectric on Ge,[24–27] however, most of the work for TiO_2 integration with Ge has been limited to (100)Ge. To the best of our knowledge, there is only one experimental report on the TiO_2/Ge band-offset; however, there is no indication of the orientation of Ge.[16] There are no prior reports on the investigation of TiO_2 for gate dielectric and for MIS contact applications on (110) and (111)Ge crystallographic orientation. These different surface orientations of Ge can foster mobility enhancement and allows one to tailor the transistor device properties. Moreover, the hole mobility was found to be the highest for (110)Ge,[28] while the electron mobility was the highest for (111)Ge.[29] Post-planar CMOS era has opened the platform for Si based non-planar multi-gate structures such as fin-shaped field-effect transistors (FinFETs) which offers superior performance in terms of gate control, device scalability, and carrier transport. The drive currents in such n- and p-channel Si FinFETs can be maximized with fins oriented along the (100) and (110) sidewalls, respectively.[30,31] Similar exploitation of orientation dependent mobility enhancement will be of key significance for the future Ge based FinFET devices and will require a fundamental insight and a comprehensive assessment of the band alignment at the TiO_2/Ge heterointerface for the different orientations of Ge. Thus, one purpose of this article is to evaluate the feasibility of employing TiO_2 as a potential high-κ dielectric with Ge. An additional motivating factor for this study stems from the use of TiO_2 for MIS contact application with different crystallographic orientations of Ge.

In this paper, we report the material synthesis, characterization, and interfacial band alignment properties of physical vapor deposited (PVD) nanoscale TiO_2 thin films on crystallographic oriented epitaxial Ge layers, which were grown on (100), (110), and (111)A GaAs substrates by molecular beam epitaxy (MBE). Analytical analysis conducted using x-ray photoelectron spectroscopy (XPS) and spectroscopic ellipsometry provides a coherent picture of the band alignment at the TiO_2/Ge heterointerface, allowing us to critically evaluate the feasibility of employing TiO_2 as high-κ gate dielectric and for future MIS contact applications with different crystallographic orientated Ge. These band alignment parameters will provide a key insight into the potential leakage current mechanisms and to further explore the integration of TiO_2 with next generation Ge MOSFET and FinFET device applications.

II. EXPERIMENTAL

A. Material synthesis

Epitaxial Ge layers were grown on epi-ready polar (100)GaAs, nonpolar (110)GaAs, and polar (111)A GaAs substrates using dual chamber (III-V and Ge) solid source MBE cluster connected via ultra-high vacuum transfer chamber. Following the oxide desorption of GaAs substrates in the III-V chamber, the respective substrates were transferred to the Ge MBE chamber. The epitaxial Ge layers, ~80 nm in thickness, were grown at a growth temperature of ~400 °C. The detailed growth procedure is reported elsewhere.[32] For synthesizing TiO_2 pellets, we employed the conventional solid-state reaction method. Commercial rutile phase TiO_2 powder (Alfa Aesar, 99.9% purity) was first uniaxially pressed into the target followed by cold isostatic pressing to achieve high green density. Thereafter, this target was sintered at 1350 °C (heating/cooling rate 10 °C/min) for 10 h to get highly dense ceramic body which were employed as source pellets during PVD deposition.

Prior to loading each Ge/GaAs substrate into the PVD chamber for TiO_2 deposition, each of the crystallographic oriented epitaxial Ge substrate was cleaned in NH_4OH:H_2O_2:H_2O (2:1:1000 by volume ratio) wet chemistry for 5 s, followed by a rinse in DI water and were subsequently blown dried in nitrogen. The queue time between substrate cleaning and loading into the PVD chamber was minimized to avoid subsequent air exposure. Nanoscale TiO_2 thin films with thicknesses of ~25 nm and ~1.5 nm were deposited at a substrate temperature of 250 °C using the electron-beam PVD technique. A chamber base pressure of $\sim 10^{-6}$ Torr was realized for the TiO_2 deposition. Ultra-high pure oxygen gas was introduced as the process gas with a delay of about 30 s after starting the TiO_2 deposition in order to substitute the loss of oxygen that could have resulted from the source heating by the electron-beam. Table I provides an overview of the key PVD process parameters employed during the nanoscale TiO_2 film deposition.

B. Material characterization

Cross-sectional transmission electron microscopy (TEM) was performed using the FEI Titan 80–300 transmission electron microscope to inspect the microstructure and the interface quality and to confirm the thickness of the respective layers. TEM samples were prepared by the conventional mechanical grinding and dimpling procedure followed by Ar^+ ion milling. To investigate the structure of the synthesized TiO_2 pellets, X-ray diffraction (XRD) pattern were recorded using a PANalytical X'Pert Pro powder X-ray diffractometer (Cu Kα radiation) at an operating voltage of 45 kV and a current of 40 mA, for 2θ values ranging from 20° to 60°. The band-gap of TiO_2 was determined from the Tauc's method[33] using variable angle spectroscopic ellipsometry. Photon-energy-dependent ellipsometry spectra Δ and φ were measured using a 5 nm increment from 300 nm to 800 nm. The band alignment for TiO_2 with respect to different crystallographic orientations of Ge was investigated

TABLE I. Process parameters employed during deposition of TiO_2 thin films using electron beam physical vapor deposition (PVD).

PVD process parameters	Value
Chamber base pressure	$\sim 10^{-6}$ Torr
Oxygen flow rate	5 sccm
Deposition temperature	250 °C
Substrate rotation speed	5 rpm
Deposition rate	~0.4–0.5 Å/s

using a PHI Quantera SXM XPS system equipped with a monochromatic Al-$K\alpha$ x-ray source. A pass energy of 26 eV and an exit angle of 45° were used during the measurement. Charge neutralization was taken into account, and all the XPS spectra were calibrated by adjusting the carbon 1s core-level peak position to 285 eV. Initially, the sample surface was examined by low-resolution survey scans to determine the elements present, followed by the collection of high-resolution spectra for the Ge3d and Ti3p core-levels and their respective valence band maxima (VBM). Curve fitting was performed with the CasaXPS 2.3.14 using a Lorentzian convolution with Shirley-type background. The VBM values were extracted by the linear extrapolation of the leading edge to the base line of the respective valence band spectra for the thick-TiO_2 and Ge layers.

III. RESULTS AND DISCUSSION

A. Material characterization

XRD measurements were performed for the phase characterization of the synthesized TiO_2 pellets prior to the thin film PVD deposition. Figure 1 shows the powder XRD pattern of the TiO_2 pellet which was synthesized using the conventional solid-state reaction method. Indexing of the observed diffractions peaks corresponds to the rutile phase of TiO_2, as evident from the XRD pattern. This rutile phase observed in the TiO_2 pellet was attributed to the high temperature sintering process employed during the synthesis of TiO_2 pellets. Interestingly, when the TiO_2 films were deposited on crystallographic oriented epitaxial Ge using PVD process at 250 °C, the distinct peaks corresponding to the rutile phase were not detected on the thin film samples. Thus, it can be inferred that TiO_2 thin film deposited by PVD was amorphous in nature. This observation is also consistent with prior studies on the amorphous nature of TiO_2 thin films realized during deposition at low substrate temperatures.[34–36] The amorphous TiO_2 has been shown to exhibit dielectric constant of ~50 (Ref. 25) which is about 2.5× higher than the dielectric constant of HfO_2 (~20), the state-of-the-art gate dielectric for Si-based metal-oxide-semiconductor (MOS) devices.[24]

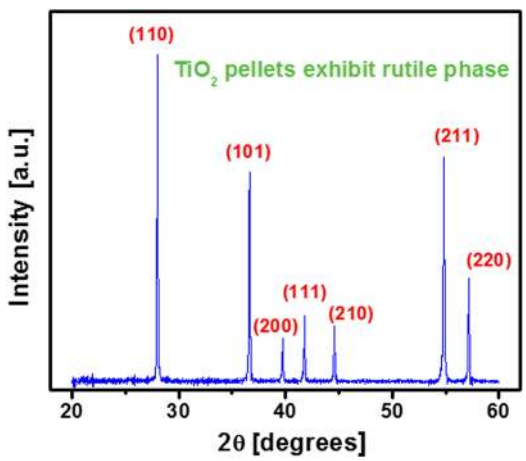

FIG. 1. Powder X-ray diffraction pattern revealing rutile phase of TiO_2 pellets synthesized by conventional solid-state reaction method.

It has been widely reported that the unwanted interfacial Ge oxide layer (GeO_x) formed between the high-κ dielectric and the Ge layer has a detrimental impact on the transistor performance pertaining to its low dielectric constant ($\kappa = 3.0$–3.8)[37] and to its poor chemical and thermal stability.[7] In order to gain insight into the structural quality and to examine the presence of any unwanted interfacial layers at the interface of TiO_2 and the epitaxial (110)Ge, the cross-sectional TEM measurement was performed. The TEM micrograph in Figure 2(a) illustrates a uniform thickness of ~25 nm for the physical vapor deposited TiO_2 thin films with well-defined and nearly abrupt interface between the TiO_2 and the epitaxial (110)Ge layer. The corresponding high-resolution TEM micrograph in Figure 2(b) reveals that no interfacial GeO_x layer was present between the TiO_2 thin film and the epitaxial Ge, indicative of a robust interface that prevents the oxidation of (110)Ge surface. We believe that the pre-cleaning of the epitaxial Ge samples in a NH_4OH:H_2O_2:H_2O wet etch chemistry along with minimizing the transfer time to the PVD chamber provides a promising method for realizing interfacial oxide-free TiO_2/Ge heterojunctions. Utilizing a similar pre-clean method, we have recently demonstrated an interfacial oxide-free heterointerface for atomic layer deposited Al_2O_3,[38] HfO_2,[39] and pulse laser deposited $BaTiO_3$ (Ref. 40) on epitaxial Ge. In addition, the TEM micrographs also confirmed that the physical vapor deposited TiO_2 thin films were amorphous in nature, as apparent from Figure 2(b), further confirming the XRD results on the amorphous nature of TiO_2 thin films.

The optical band-gap of TiO_2 was determined from the commonly used Tauc's method[33] which relates the energy dependence of the material to its absorption coefficient near the absorption edge by the following expression:

$$(\alpha\hbar\upsilon)^{1/2} = A(\hbar\upsilon - E_o), \tag{1}$$

where α is the absorption coefficient, $\hbar\nu$ is the incident photon energy, and A is a constant. Figure 3(a) shows the Tauc plot for indirect transition ($(\alpha\hbar\upsilon)^{1/2}$ versus $\hbar\upsilon$) for the 25 nm thick TiO_2 film. The optical band-gap was extracted by extending the linear section of the plot to intersect the x-axis, and the band-gap was extrapolated as 3.33 ± 0.02 eV. Several different lines were drawn to linearly fit the slope in Tauc's plot, all of these lines were extrapolated to intersect the x-axis to determine the band-gap, and an uncertainty of ± 0.02 eV was obtained. This band-gap is used in Sec. III B to calculate the CBOs from the experimentally determined valence band-offsets (VBOs or ΔE_v) from XPS.

B. Energy band alignment of TiO_2/Ge heterointerface

The physical insight into the energy band alignment at the TiO_2/Ge heterointerface is of key significance to investigate the feasibility of TiO_2 as an effective gate dielectric on Ge and for its application to realize MIS contacts on Ge. XPS technique allows the direct measurement of the ΔE_v at the TiO_2/Ge heterointerface for the three crystallographic oriented (100), (110), and (111)Ge layers by measuring the binding energy from the core levels (CLs) of Ge3d and Ti3p

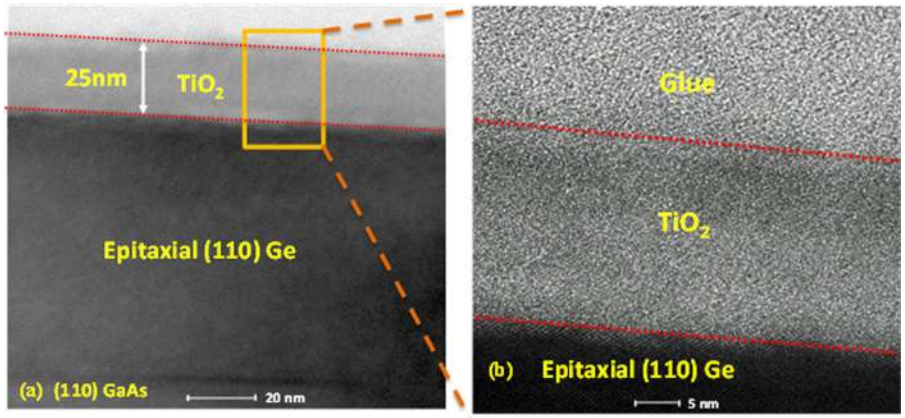

FIG. 2. (a) Cross-sectional TEM micrograph of TiO_2 thin films deposited on epitaxial Ge grown on (110)GaAs substrate. (b) High-resolution TEM micrograph corresponding to the highlighted region in (a) shows an abrupt interface between TiO_2 thin film and epitaxial Ge and confirms the amorphous nature of PVD deposited TiO_2 thin film at 250 °C.

and the VBM of TiO_2 and Ge, respectively. During the XPS measurement, we used continuous flow of electrons to minimize the binding energy shift caused due to the charging effects. All the respective binding energies were corrected by adjusting the carbon 1s core-level peak position to 285.0 eV during each sample analysis. The CL energy positions for all the peaks were defined at the full-width at half-maximum for the respective peak. The prime source of error in VBO measurements using XPS is during the precise fitting to obtain the VBM by linear extrapolation method from the intersection of the linear section of the valence band (VB) leading edge to the linear fit of the background.[41] This extrapolation method is sensitive to the point considered on the leading edge of the valence band spectra to obtain the regression line. The precise determination of band offset of a heterostructure is determined by the linearity and stability of the energy scale and not the energy resolution. In our study, the binding energy difference between different elements or different binding energy levels of one element is much larger than the energy resolution of our XPS system (0.45 eV with pass energy 26 eV). Hence, the energy resolution was not a limitation of our study. The stability and repeatability of the XPS system is more important which determines the peak value fluctuation between different measurements. The error bar we defined in this paper is due to the scatter of valence band spectra during the fitting of VBM position and considering the linearity and stability of the energy scale of the XPS binding energy spectrum and it is typically less than 0.03 eV based on the statistical measurement of a peak position of the PHI SXM XPS system. Several different set of points were selected over the linear region of the leading edge, and linear region of the background to perform regressions and hence an uncertainty of ±0.05 eV has been included in the experimentally determined VBO values to reflect the errors involved during this extrapolation method.

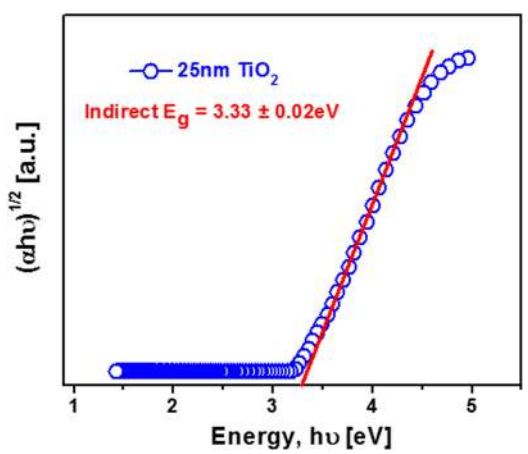

FIG. 3. Tauc plot for $(\alpha\hbar\upsilon)^{1/2}$ versus $\hbar\upsilon$ corresponding to indirect transition for TiO_2 thin films.

For each crystallographic Ge orientation, the XPS spectra were collected from three samples: (1) 80 nm thick epitaxial Ge sample to measure the CL binding energy and the VBM of Ge, (2) 25 nm thick TiO_2 on Ge (hereafter referred as thick-TiO_2) to measure the CL binding energy of Ti and the VBM of TiO_2, and (3) 1.5 nm thick TiO_2 on Ge (hereafter referred as thin-TiO_2) to measure the CL binding energy of Ti and Ge at the TiO_2/Ge heterointerface. Utilizing the binding energy information from these respective samples, the VBOs at the TiO_2/Ge heterointerface for each orientation were determined from Kraut's method using the following equation:[42]

$$\Delta E_V = \left(E^{Ge}_{Ge3d} - E^{Ge}_{VBM}\right)^{Ge} - \left(E^{Ti}_{Ti3p} - E^{Ti}_{VBM}\right)^{Think-Tio_2} - \Delta E_{CL}(i)^{Thin-Tio_2}, \quad (2)$$

where $\left(E^{Ge}_{Ge3d}\right)$ and $\left(E^{Ti}_{Ti3p}\right)$ are the CL binding energies of Ge3d and Ti3p; $\left(E^{Ge}_{VBM}\right)$ and $\left(E^{Ti}_{VBM}\right)$ are the VBM of epitaxial Ge and thick-TiO_2 samples, and $\Delta E_{CL}(i) = \left(E^{Ge}_{Ge3d}(i) - E^{Ti}_{Ti3p}(i)\right)$ represents the binding energy difference between the Ge3d and Ti3p core-levels, measured at the heterointerface from the 1.5 nm TiO_2 on Ge sample for each crystallographic orientation.

Figure 4(a) shows the Ti3p CL and VB spectra for the thick-TiO_2 film, and Figure 4(b) shows the respective Ti3p CL $\left(E^{Ti}_{Ti3p}\right)$ and Ge3d CL $\left(E^{Ge}_{Ge3d}\right)$ spectra for the thin-TiO_2 film grown on (100)Ge. The corresponding CL and VB spectra for the thick-TiO_2 and thin-TiO_2 films grown on (110)Ge and (111)Ge are illustrated in Figures 5 and 6, respectively. Utilizing the method described above, the corresponding binding energy difference between the Ge3d CL peak and the VBM $\left(E^{Ge}_{Ge3d} - E^{Ge}_{VBM}\right)$ for the three crystallographic oriented Ge layers were determined to be 29.45 ± 0.05 eV for (100)Ge, 29.36 ± 0.05 eV for (110)Ge, and 29.58 ± 0.05 eV

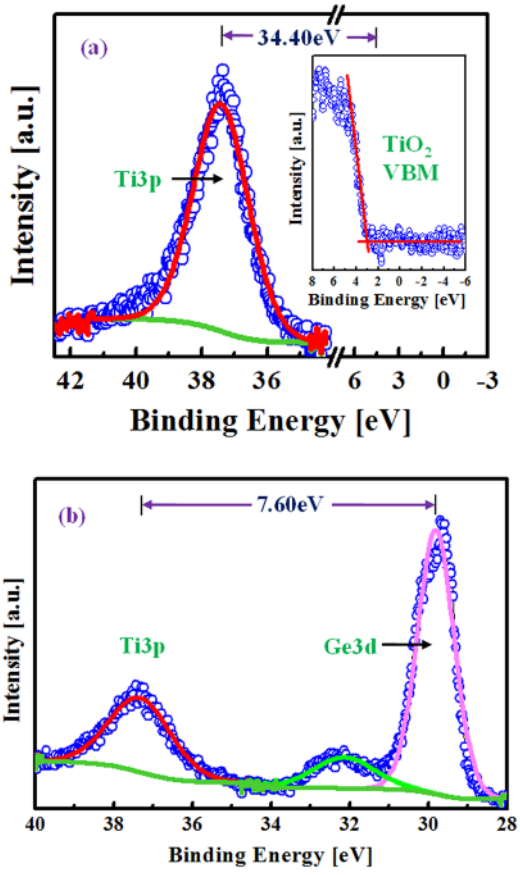

FIG. 4. XPS spectra of (a) Ti3p (E^{Ti}_{Ti3p}) core level with the inset showing the VBM (E^{Ti}_{VBM}) from 25 nm thick TiO_2 film and (b) Ti3p (E^{Ti}_{Ti3p}), Ge3d (E^{Ge}_{Ge3d}) core level peaks from 1.5 nm TiO_2 film on (100)Ge interface.

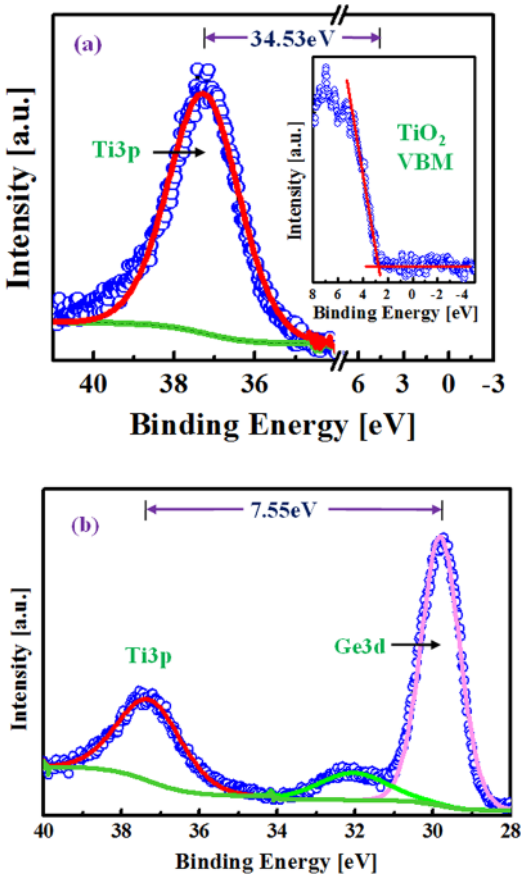

FIG. 5. XPS spectra of (a) Ti3p (E^{Ti}_{Ti3p}) core level with the inset showing the VBM (E^{Ti}_{VBM}) from 25 nm thick TiO_2 film, and (b) Ti3p (E^{Ti}_{Ti3p}), Ge3d (E^{Ge}_{Ge3d}) core level peaks from 1.5 nm TiO_2 film on (110)Ge interface.

for (111)Ge, respectively, as reported earlier.[39] The thickness of epitaxial Ge for these measurements were ~80 nm, which was sufficiently thick for XPS analysis since most of the signal in XPS measurement is from within the first 1–10 nm of the sample thickness. The CL to VBM binding energy difference obtained for the thick-TiO_2 film $(E^{Ti}_{Ti3p} - E^{Ti}_{VBM})$ and for the epitaxial Ge $(E^{Ge}_{Ge3d} - E^{Ge}_{VBM})$ along with the binding energy difference between the Ti3p CL and Ge3d CL peak $(E^{Ge}_{Ge3d}(i) - E^{Ti}_{Ti3p}(i))$ at the thin-TiO_2/Ge heterointerface for the three crystallographic oriented epitaxial (100), (110), and (111)Ge layers are summarized in Tables II–IV, respectively. Utilizing these measured differences in the binding energies in Eq. (2) (also reported in Tables II–IV), the measured VBOs for TiO_2 relative to epitaxial (100)Ge, (110)Ge, and (111)Ge were determined to be 2.65 ± 0.05 eV, 2.38 ± 0.05 eV, and 2.48 ± 0.05 eV, respectively. The corresponding CBOs, ΔE_c, for the respective crystallographic orientation were calculated using the following equation:

$$\Delta E_C = E_g^{TiO_2} - E_g^{Ge} - \Delta E_V, \tag{3}$$

where $E_g^{TiO_2}$ and E_g^{Ge} are the respective band-gaps of TiO_2 and Ge. The band-gap used for Ge was 0.67 eV while a measured band-gap of 3.33 ± 0.02 eV was utilized for the TiO_2. The calculated CBOs for TiO_2 relative to epitaxial (100)Ge, (110)Ge, and (111)Ge were determined to be 0.01 ± 0.07 eV, 0.28 ± 0.07 eV, and 0.18 ± 0.07 eV, respectively. These CBOs are calculated by taking into account the errors associated from the band-gap extrapolation using Tauc's method. The schematic band alignment diagrams

TABLE II. Core-level to VBM, and interface core-level binding-energy differences for TiO_2 and epitaxial (100)Ge grown on (100)/6° GaAs substrate.

		Band offsets of TiO_2/(100)Ge	
Material and interface	Binding energy difference	Measured ΔE_V (eV)	Calculated ΔE_C (eV)
Ge	$E^{Ge}_{Ge3d} - E^{Ge}_{VBM} = 29.45 \pm 0.05$eV[a]		
25 nm TiO_2	$E^{Ti}_{Ti3p} - E^{Ti}_{VBM} = 34.40 \pm 0.05$eV		
1.5 nm TiO_2 on Ge	$E^{Ti}_{Ti3p} - E^{Ge}_{Ge3d} = 7.60$eV		
E_g of TiO_2	3.33 ± 0.02 eV	2.65 ± 0.05	0.01 ± 0.07

[a]Denotes values adapted from Ref. 39.

TABLE III. Core-level to VBM, and interface core-level binding energy difference for TiO_2 and epitaxial (110)Ge grown on (110)GaAs substrate.

		Band offsets of TiO_2/(110)Ge	
Material and interface	Binding energy difference	Measured ΔE_V (eV)	Calculated ΔE_C (eV)
Ge	$E^{Ge}_{Ge3d} - E^{Ge}_{VBM} = 29.36 \pm 0.05$eV[a]		
25 nm TiO_2	$E^{Ti}_{Ti3p} - E^{Ti}_{VBM} = 34.53 \pm 0.05$eV		
1.5 nm TiO_2 on Ge	$E^{Ti}_{Ti3p} - E^{Ge}_{Ge3d} = 7.55$eV		
E_g of TiO_2	3.33 ± 0.02 eV	2.38 ± 0.05	0.28 ± 0.07

[a]Denotes values adapted from Ref. 39.

TABLE IV. Core-level to VBM, and interface core-level binding-energy difference for TiO_2 and epitaxial (111)Ge grown on (111)A GaAs substrate.

		Band offsets of TiO_2/(111)Ge	
Material and interface	Binding energy difference	Measured ΔE_V (eV)	Calculated ΔE_C (eV)
Ge	$E^{Ge}_{Ge3d} - E^{Ge}_{VBM} = 29.58 \pm 0.05$eV[a]		
25 nm TiO_2	$E^{Ti}_{Ti3p} - E^{Ti}_{VBM} = 34.60 \pm 0.05$eV		
1.5 nm TiO_2 on Ge	$E^{Ti}_{Ti3p} - E^{Ge}_{Ge3d} = 7.50$eV		
E_g of TiO_2	3.33 ± 0.02 eV	2.48 ± 0.05	0.18 ± 0.07

[a]Denotes values adapted from Ref. 39.

representative of the VBOs and the CBOs for TiO_2 films grown on (100), (110), and (111)Ge epitaxial layers are shown in Figures 7(a)–7(c), respectively, and the corresponding band-offset values are summarized in Table V. Figure 8 illustrates the representative histograms of the VBOs and CBOs for the TiO_2 relative to the (100), (110), and (111)Ge epitaxial layers. Thus, a comparative assessment on the effect of substrate orientation on the band alignment at the TiO_2/Ge interface revealed a valence band-offset relation of $\Delta E_V(100) > \Delta E_V(111) > \Delta E_V(110)$ and a conduction band-offset relation of $\Delta E_C(110) > \Delta E_C(111) > \Delta E_C(100)$. Prior research on high-κ dielectrics have indicated a dependence of substrate orientation on the band-offset at the high-κ/semiconductor interface.[38,39] It has been reported that several other parameters, namely, deposition conditions, crystallinity, interface dipole, and inter-diffusion could be responsible for the discrepancies observed in the band alignment values.[43] Band alignment, in principle, can be tuned by changing the chemical structure of the interface.[44] In context to our report, we attribute the difference in the band-offsets for different crystallographic Ge orientation to the differences in the surface reconstruction of Ge grown on different orientations of GaAs substrate.[32]

It is worth noting that the VBOs for TiO_2 relative to Ge were found to be greater than 2 eV irrespective of the Ge crystallographic orientation, indicating sufficient band-offset

TABLE V. Band-offset values of TiO_2 on crystallographic oriented epitaxial Ge layers.

	(100)	(110)	(111)
ΔE_V (eV)	2.65 ± 0.05	2.38 ± 0.05	2.48 ± 0.05
ΔE_C (eV)	0.01 ± 0.07	0.28 ± 0.07	0.18 ± 0.07

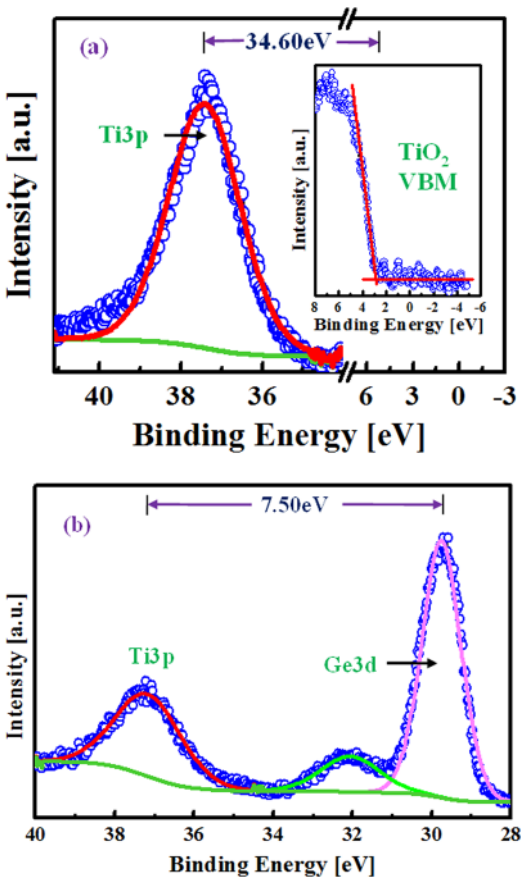

FIG. 6. XPS spectra of (a) Ti3p (E^{Ti}_{Ti3p}) core level with the inset showing the VBM (E^{Ti}_{VBM}) from 25 nm thick TiO_2 film, and (b) Ti3p (E^{Ti}_{Ti3p}), Ge3d (E^{Ge}_{Ge3d}) core level peaks from 1.5 nm TiO_2 film on (111)Ge interface.

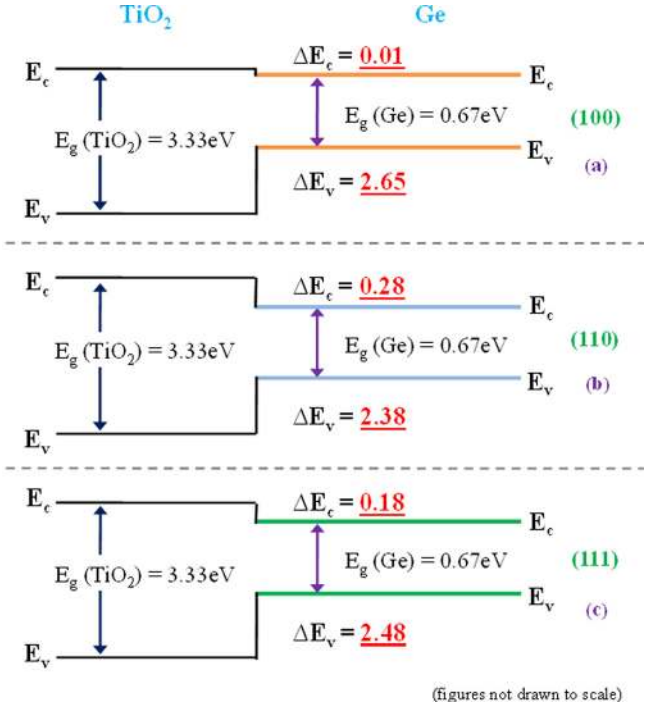

FIG. 7. Schematic energy band alignment of TiO_2 thin films on (a) (100)Ge, (b) (110)Ge, and (c) (111)Ge heterojunctions obtained from XPS and spectroscopic ellipsometry measurements.

for suppressing the hole tunneling leakage current between the TiO_2 high-κ dielectric and the Ge channel. On the contrary, the corresponding CBOs for TiO_2 relative to all the three Ge orientations were determined to be significantly smaller than 1 eV, correlating that TiO_2 provides an insufficient barrier for suppressing the electron tunneling leakage current, thus rendering the use of standalone TiO_2 dielectric as inefficient for integration with Ge channel. In order to efficiently leverage TiO_2 as the high-κ dielectric for integration with next generation low-power Ge MOSFETs, it would be imperative to focus efforts on composite oxides which would

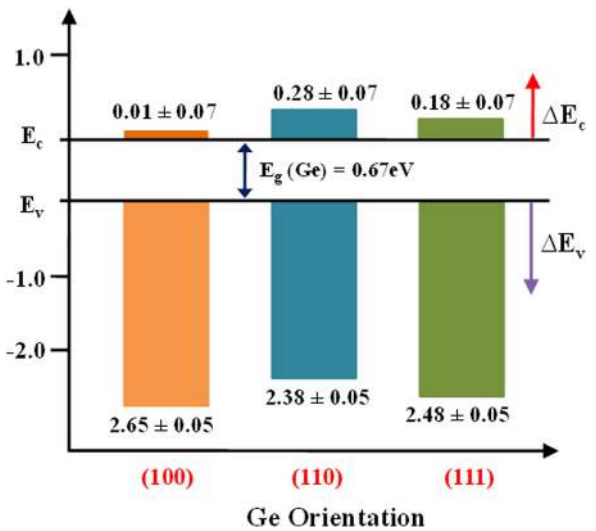

FIG. 8. Histogram of band-offset values of TiO_2 thin films on crystallographic oriented epitaxial (100)Ge, (110)Ge, and (111)Ge layers. The ΔE_V are directly measured from XPS measurement and the ΔE_C are calculated using ΔE_V and E_g; hence, the different error bars are indicated.

employ a wider band-gap bottom oxide layers with sufficient CBO to Ge such as Al_2O_3 (Refs. 24 and 38) and HfO_2.[25,39] Interestingly, the low CBOs obtained for the aforementioned TiO_2/Ge system, irrespective of the Ge crystallographic orientation presents the possibility of employing TiO_2 insulating layer in MIS contact applications to enable low specific resistance ohmic contacts to n-type Ge. This application will find key significance to realize ohmic contacts to Ge in the next generation of Ge FinFETs, where different Ge orientations can be exploited to facilitate mobility enhancement for n- and p-channel devices.

IV. CONCLUSION

In summary, the dependence of substrate orientation on band alignment at the TiO_2/Ge heterointerfaces were investigated, where the epitaxial Ge layers were grown on (100), (110), and (111)A GaAs substrate using molecular beam epitaxy. The cross-sectional TEM micrographs confirmed a sharp interface between the TiO_2 and the (110)Ge with no traceable interfacial layer. Together, XPS and spectroscopic ellipsometry were used to determine the band alignment at the TiO_2/Ge heterointerface. A comparative assessment on the effect of substrate orientation revealed a valence band-offset relation of $\Delta E_V(100) > \Delta E_V(111) > \Delta E_V(110)$ and a conduction band-offset relation of $\Delta E_C(110) > \Delta E_C(111) > \Delta E_C(100)$. Irrespective of the crystallographic orientation of epitaxial Ge layers, valence band-offsets in excess of 2 eV were measured at the TiO_2/Ge heterointerface. The corresponding conduction band-offsets were found to be sufficiently low, rendering the use of standalone TiO_2 dielectric as inefficient for integration with Ge channel, thus making it imperative to use TiO_2 in a composite dielectric configuration with Ge. Furthermore, the low CBOs will allow the implementation of TiO_2 for achieving low resistance ohmic contacts to n-Ge source/drain regions and facilitate higher on-current in next generation of Ge-based MOSFET and FinFET devices. These experimentally determined band-offset parameters and the interfacial properties of TiO_2 will provide key insight into the potential mechanism for leakage current and will also provide a valuable aid for the design and advancement of next generation Ge-based MOS devices.

ACKNOWLEDGMENTS

This work was supported in part by National Science Foundation under Grant No. ECCS-1348653 and Intel Corporation. S.P., D.M., and R.V. acknowledge the financial support from Office of Basic Energy Science, Department of Energy, through Grant No. DE-FG02-06ER46290.

[1]C. O. Chui, H. Kim, D. Chi, B. B. Triplett, P. C. McIntyre, and K. C. Saraswat, in *IEEE Conference Proceedings of International Electron Devices Meeting (IEDM)* (IEEE, 2002), p. 437.
[2]M. L. Lee, C. W. Leitz, Z. Cheng, A. J. Pitera, T. Langdo, M. T. Currie, G. Taraschi, E. A. Fitzgerald, and D. A. Antoniadis, Appl. Phys. Lett. **79**, 3344 (2001).
[3]Q. Xie, S. Deng, M. Schaekers, D. Lin, M. Caymax, A. Delabie, X.-P. Qu, Y.-L. Jiang, D. Deduytsche, and C. Detavernier, Semicond. Sci. Technol. **27**, 074012 (2012).

[4]T. Irisawa, T. Numata, T. Tezuka, K. Usuda, S. Nakaharai, N. Hirashita, N. Sugiyama, E. Toyoda, and S. Takagi, in *IEEE Conference Proceedings of International Electron Devices Meeting (IEDM)* (IEEE, 2005), p. 709.
[5]T. Takahashi, T. Nishimura, L. Chen, S. Sakata, K. Kita, and A. Toriumi, in *IEEE Conference Proceedings of International Electron Devices Meeting (IEDM)* (IEEE, 2007), p. 697.
[6]T. Yamamoto, Y. Yamashita, M. Harada, N. Taoka, K. Ikeda, K. Suzuki, O. Kiso, N. Sugiyama, and S. Takagi, in *IEEE Conference Proceedings of International Electron Devices Meeting (IEDM)* (IEEE, 2007), p. 1041.
[7]A. Delabie, F. Bellenger, M. Houssa, T. Conard, S. Van Elshocht, M. Caymax, M. Heyns, and M. Meuris, Appl. Phys. Lett. **91**, 082904-1 (2007).
[8]G. D. Wilk, R. M. Wallace, and J. M. Anthony, J. Appl. Phys. **89**, 5243 (2001).
[9]J. Robertson, J. Vac. Sci. Technol. B **18**, 1785 (2000).
[10]J. Robertson, Eur. Phys. J. Appl. Phys. **28**, 265 (2004).
[11]Y.-C. Yeo, T.-J. King, and C. Hu, Appl. Phys. Lett. **81**, 2091 (2002).
[12]A. Dimoulas, P. Tsipas, A. Sotiropoulos, and E. K. Evangelou, Appl. Phys. Lett. **89**, 252110 (2006).
[13]T. Nishimura, K. Kita, and A. Toriumi, Appl. Phys. Lett. **91**, 123123 (2007).
[14]Y. Zhou, M. Ogawa, X. Han, and K. L. Wang, Appl. Phys. Lett. **93**, 202105 (2008).
[15]M. Kobayashi, A. Kinoshita, K. Saraswat, H.-S. P. Wong, and Y. Nishi, J. Appl. Phys. **105**, 023702 (2009).
[16]J. Y. Lin, A. M. Roy, A. Nainani, Y. Sun, and K. C. Saraswat, Appl. Phys. Lett. **98**, 092113-1 (2011).
[17]P. P. Manik, R. K. Mishra, V. P. Kishore, P. Ray, A. Nainani, Y.-C. Huang, M. C. Abraham, U. Ganguly, and S. Lodha, Appl. Phys. Lett. **101**, 182105 (2012).
[18]J. Tang, Y. Wu, E. W. McFarland, and G. D. Stucky, Chem. Commun. **2004**, 1670.
[19]B. Tan and Y. Wu, J. Phys. Chem. B **110**, 15932 (2006).
[20]M. Ni, M. K. Leung, D. Y. Leung, and K. Sumathy, Renewable Sustainable Energy Rev. **11**, 401 (2007).
[21]X. Zhang, A. Fujishima, M. Jin, A. V. Emeline, and T. Murakami, J. Phys. Chem. B **110**, 25142 (2006).
[22]E. Ceresa, L. Burlamacchi, and M. Visca, J. Mater. Sci. **18**, 289 (1983).
[23]Y. Zhu, J. Shi, Z. Zhang, C. Zhang, and X. Zhang, Anal. Chem. **74**, 120 (2002).
[24]S. Swaminathan, M. Shandalov, Y. Oshima, and P. C. McIntyre, Appl. Phys. Lett. **96**, 082904-1 (2010).
[25]Q. Xie, D. Deduytsche, M. Schaekers, M. Caymax, A. Delabie, and X.-P. Qu, Appl. Phys. Lett. **97**, 112905-1 (2010).
[26]Q. Xie, J. Musschoot, M. Schaekers, M. Caymax, A. Delabie, D. Lin, X.-P. Qu, Y.-L. Jiang, S. V. den Berghe, and C. Detavernier, Electrochem. Solid State Lett. **14**, G27 (2011).
[27]P. Ardalan, E. R. Pickett, J. J. S. Harris, A. F. Marshall, and S. F. Bent, Appl. Phys. Lett. **92**, 252902 (2008).
[28]J. H. Choi, Y. Mao, and J. P. Chang, Mater. Sci. Eng. R **72**, 97 (2011).
[29]T. Krishnamohan, D. Kim, T. V. Dinh, A. T. Pham, B. Meinerzhagen, C. Jungemann, and K. C. Saraswat, in *IEEE Conference Proceedings of International Electron Devices Meeting (IEDM)* (IEEE, 2008), p. 899.
[30]J. Kavalieros, B. Doyle, S. Datta, G. Dewey, M. Doczy, B. Jin, D. Lionberger, M. Metz, W. Rachmady, M. Radosavljevic, U. Shah, N. Zelick, and R. Chau, in *IEEE Symposium on VLSI Technology (VLSI)* (IEEE, 2006), p. 50.
[31]L. Chang, Y.-K. Choi, D. Ha, P. Ranade, S. Xiong, J. Bokor, C. Hu, and T.-J. King, Proc. IEEE **91**, 1860 (2003).
[32]M. K. Hudait, Y. Zhu, N. Jain, and J. L. Hunter, Jr., J. Vac. Sci. Technol. B **31**, 011206-1 (2013).
[33]J. Tauc, R. Grigorovici, and A. Vancu, Phys. Status Solidi B **15**, 627 (1966).
[34]P. Löbl, M. Huppertz, and D. Mergel, Thin Solid Films **251**, 72 (1994).
[35]T.-S. Yang, C. B. Shiu, and M. S. Wong, Surf. Sci. **548**, 75 (2004).
[36]R. van de Krol and A. Goossens, J. Vac. Sci. Technol. A **21**, 76 (2003).
[37]S. J. Lee, C. Zhu, and D. L. Kwong in *Advanced Gate Stacks for High-Mobility Semiconductors*, edited by A. Dimoulas, E. Gusev, P. C. McIntyre, and M. Heyns (Springer, Berlin, 2007).
[38]M. K. Hudait, Y. Zhu, D. Maurya, S. Priya, P. K. Patra, A. W. K. Ma, A. Aphale, and I. Macwan, J. Appl. Phys. **113**, 134311-1 (2013).
[39]M. K. Hudait and Y. Zhu, J. Appl. Phys. **113**, 114303-1 (2013).
[40]M. K. Hudait, Y. Zhu, N. Jain, D. Maurya, Y. Zhou, and S. Priya, J. Appl. Phys. **114**, 024303-1 (2013).
[41]S. A. Chambers, T. Droubay, T. C. Kaspar, and M. Gutowski, J. Vac. Sci. Technol. B **22**, 2205 (2004).
[42]E. A. Kraut, R. W. Grant, J. R. Waldrop, and S. P. Kowalczyk, Phys. Rev. Lett. **44**, 1620 (1980).
[43]L. J. Brillson, *Surfaces and Interfaces of Electronic Materials* (Wiley-VCH, Germany, 2010).
[44]M. Perego, G. Seguini, G. Scarel, M. Fanciulli, and F. Wallrapp, J. Appl. Phys. **103**, 043509-1 (2008).